International Journal of Environmental Science and Technology (2022) 19:4167–4180
https://doi.org/10.1007/s13762-021-03592-9

ORIGINAL PAPER

Biopolymer-based adsorptive membrane for simultaneous removal of cationic and anionic heavy metals from water

E. Shokri[1] · B. Khanghahi[2] · E. Esmizadeh[2] · H. Etemadi[2]

Received: 26 April 2021 / Revised: 26 July 2021 / Accepted: 30 July 2021 / Published online: 4 September 2021

Abstract

In this study, a biopolymer-based adsorptive membrane was designed for simultaneous removal of differently charged heavy metals from water. Polylactic acid (PLA)/hydroxyapatite (HAp) adsorptive membranes with various content of HAp were fabricated using the non-solvent induced phase separation method. The effect of incorporating different weight content of HAp ranging from 0 to 3.0 wt% was studied on the structural morphology, hydrophilicity, porosity, mechanical properties, pure water permeability, and lead (Pb) and arsenic (As) adsorption capacity of the fabricated membranes. The results revealed that adsorptive membrane with 2.5 wt% HAp exhibited high porosity and hydrophilicity, acceptable mechanical strength, and ultrahigh pure water flux (1100 L m^{-2} h^{-1}). This membrane showed proper removal efficiency in batch adsorption, 97% for Pb and 82% for As solutions (100 ppb), which are comparable to most of the readily available adsorbents. Dynamic adsorption results divulged that the adsorptive membrane with 2.5 wt% HAp content provided a promising filtrate of Pb and As solutions with a concentration below 10 ppb for even four and five consequent regeneration cycles. Additionally, the adsorptive performance of the optimum HAp content membrane was better than batch adsorption, especially in Pb removal.

Keywords Adsorptive membrane · Hydroxyapatite · Polylactic acid · Lead · Arsenic

Abbreviations

TMP	Transmembrane pressure
PWF	Pure water flux
HAp	Hydroxyapatite
PLA	Polylactic acid
As	Arsenic
Pb	Lead
Zn	Zinc
Cu	Copper
Cd	Cadmium
Co	Cobalt
Ni	Nickel
Cr	Chromium
Se	Selenium
FE-SEM	Field emission scanning electron microscope
AFM	Atomic force microscopy
FTIR	Fourier transform infrared spectroscopy
EDX	Energy-dispersive X-ray spectroscopy
DI	Deionized
CA	Contact angle
NMP	*N*-Methyl-2-pyrrolidone
WHO	World Health Organization
ppb	One part per billion
ppm	One part per million

Introduction

Over the last decade, a shortage of safe drinking water is becoming a serious concern worldwide for public health that causes much attention to be paid to various drinking water treatment measures. Among the various pollutants in water, heavy metals are non-biodegradable and highly toxic even at low concentrations (Chon et al. 2010; Fu and Wang 2011). Industrial wastewater comprises varieties of heavy metals with positive or negative net charges in naturally available forms. Arsenic (As) and lead (Pb) are well-known toxic heavy metals that are discharged from various industrial processes to wastewater (Naseem and Tahir

Editorial responsibility: J. Aravind.

✉ E. Shokri
Elh.shokri@ubonab.ac.ir

[1] Department of Chemical Engineering, University of Bonab, Bonab, Iran

[2] Department of Polymer Science and Engineering, University of Bonab, Bonab, Iran

2001). In wastewater, lead exists as a cationic form (Pb^{2+}), whereas arsenic under oxidizing and aerated conditions found in its oxyanionic forms, such as $H_2AsO_4^-$, $HAsO_4^{2-}$ or AsO_4^{3-} (Dixit and Hering 2003). World Health Organization (WHO) guidelines presented that levels of As and Pb in drinking water shall not exceed 10 ppb.

Diverse methods such as precipitation/coagulation (Manica et al. 2020), photocatalysis (Damodar et al. 2009; Kıranşan et al. 2015), adsorption (Gopalakannan et al. 2018), and membrane filtration (Uddin et al. 2007; Sogaard 2014; Lee et al. 2016) are used for the heavy metal removal from drinking water. Among them, adsorptive polymer membranes which utilize inorganic additives as adsorbent have got much attention and extended in developing countries (Chatterjee and De 2015). Adsorptive membranes do not require high transmembrane pressure (TMP) that makes them more efficient option in comparison with nanofiltration and reverse osmosis (Abdullah et al. 2016). Heavy metal ions from wastewater can be adsorbed by charged inorganic materials incorporated in the membrane through electrostatic interaction. However, most of the adsorbents are not able to adsorb the positively and negatively charged heavy metal ions simultaneously. Feasible approaches to enhance the simultaneous adsorption of cationic and anionic heavy metals are to functionalize the raw adsorbents or synthesis of nanocomposites. Nonetheless, the main drawback of the former method is the need for using highly pure organic reagents, which are considerably expensive and toxic.

This technology faces challenges since the toxicity of the nanoparticles in adsorptive membranes will bring serious pollution after recycling these membranes for multiple adsorption–desorption cycles. In this perspective, it is critically important to incorporate environmentally friendly nanoparticles such as natural bio-based materials with adsorptive sites for cationic and anionic pollutants. Hydroxyapatite $[Ca_{10}(PO_4)_6(OH)_2]$, a naturally available form of calcium phosphate, is a well-known member of these materials with high biocompatibility and essentially no toxicity (Louihi et al. 2020). Specifically, it has a hexagonal structure and calcium to phosphate ratio of 1.78, which is very similar to bone apatite (Jiang et al. 2013; Anwar and Arthanareeswaran 2019). HAp has been used for environmental applications such as efficient and selective removal of heavy metals, dyes, and other emerging pollutants from aqueous solutions due to its high surface reactivity, charge density, and also ion exchange capability (Tomar et al. 2015; Yang et al. 2015; de Resende et al. 2019). Furthermore, HAp has also been highlighted as a cost-effective and eco-friendly adsorbent. Containing both acid and basic sites in its structure, it can be concluded that HAp has a considerable potential for the removal of cationic and anionic pollutants from water (Hubadillah et al. 2020). In recent years, incorporation of natural and modified HAp either individually or as a composite with other materials has been widely reported as adsorbents for various ions including Zn (Song et al. 2008; Viipsi et al. 2013; Foroughi et al. 2015), Cu (Thanh et al. 2018; Deng et al. 2020; Pooladi and Bazargan-Lari 2020), Cd (Corami et al. 2008; Viipsi et al. 2013), Co (Sheha et al. 2016), Ni (Thanh et al. 2018), Cr (Hokkanen et al. 2016; Al-Wafi et al. 2020; Campisi et al. 2021), Pb (Saoiabi et al. 2013; RoyChoudhury et al. 2019; Anutrasakda et al. 2020; Fang et al. 2020; Jiang et al. 2020), and As (Czerniczyniec et al. 2007). Graphene oxide/magnetite/HAp/cellulose acetate nanofibrous membranes were reported to successfully eliminate Cr(VI) and Se(IV) at pH = 8 and remove 97.3% of Cr(VI) and 89.3% of Se(IV) at pH = 4 from water (Al-Wafi et al. 2020). Successful adsorption of Cu was carried out in batch mode, and the maximum adsorption capacity was 67.8 mg/g using elecrospun nano-HAp/gelatin/zein nanofibrous membranes (Deng et al. 2020). HAp clay-alumina ceramic ultrafiltration membrane was investigated by Roychoudhury et al. for Pb removal in dynamic adsorption mode. The obtained results showed maximum 99.6% Pb rejection of 5 mg L^{-1} under pressure of 1 bar (RoyChoudhury et al. 2019).

The other key parameter controlling the performance of the adsorptive membrane is the polymer matrix, which should have large water flux even at low pressure. Polylactic acid (PLA) is synthetic linear aliphatic thermoplastic polyester derived from naturally occurring organic acid (lactic acid) (Iniguez-Franco et al. 2016). The biocompatibility of PLA with the human body has led to broad and diverse applications such as tissue engineering and drug delivery (Pandele et al. 2017; Chuan et al. 2020; Fu et al. 2021). Due to its hydrophilic and non-toxic properties, PLA has recently gained attention as a promising polymer for ultrafiltration membranes (Moriya et al. 2012). Thus, PLA was chosen in the current study as the matrix of the biopolymer-based adsorptive membrane. The fabrication of PLA/HAp adsorptive membranes and their performance toward simultaneous cationic and anionic heavy metal ions removal has not yet been investigated.

In this work, a novel hybrid composite membrane based on PLA biopolymer and naturally derived HAp was developed as an adsorptive membrane for simultaneous removal of cationic and anionic heavy metals. The effect of HAp content on morphology, surface hydrophilicity, porosity, and mechanical performance of the membranes was studied. The

optimum conditioned membrane was employed for water treatment by simultaneous removal of Pb and As in both batch and dynamic adsorption modes. The isotherms and kinetic parameters were established by two-parameter models, Langmuir and Freundlich, to analyze the adsorption mechanism.

Neat and adsorptive membranes were fabricated and characterized at Department of Chemical Engineering of University of Bonab. Identification of heavy metals concentrations was performed at water and wastewater company's laboratory of East Azarbaijan. All experiments were performed between 2019 and 2021.

Materials and methods

Materials

PLA as the biopolymer matrix with a molecular weight of 60,000 g/mol was supplied by Warrington, PA_America. Hydroxyapatite nanopowders, < 200 nm particle size, were purchased from Sigma-Aldrich. *N*-Methyl-2-pyrrolidone (NMP) as the solvent was obtained from Merck, Germany. As and Pb stock solutions with concentration of 1000 ppm were prepared by dissolving appropriate amounts of sodium hydrogen arsenate and lead chloride in deionized water, respectively. Adjustment of pH was accomplished using 0.1 M NaOH or 0.1 M HCl. All of these chemicals were of analytical grade and supplied by Sigma-Aldrich, Germany.

Preparation of adsorptive membranes

All membranes were fabricated by using non-solvent induced phase separation method. Firstly, a distinct amount of PLA polymer was dried at 60 °C for 1 h and dissolved at NMP under stirring at 80 rpm for 2 h. HAp nanoparticles in various weight percentages, 0.5, 1.0, 2.0, 2.5, and 3.0 wt%, were weighed and dispersed into 5 g of NMP using ultrasonicate. Subsequently, the suspension was added to PLA solution in NMP and stirred at 40 rpm and 60 °C until a homogeneous solution was obtained (8 h). Afterward, the homogeneous solution was ultrasonicated for 15 min and then allowed to degas for 6 h. A portion of the solution was cast onto a sheet using a custom-made film applicator with a thickness of 150 µm. Immediately after casting, the film was immersed in DI water bath to initiate phase inversion and retained for 24 h. Finally, membranes were dried at room temperature for another 24 h. Table 1 summarizes the details of the solution dope compositions for the prepared membranes.

Table 1 Composition of casting solution for neat and adsorptive PLA membranes

Membrane	15 wt%		85 wt%
	HAp (wt%)	PLA (wt%)	NMP (wt%)
PLA	0.0	100	85
PLA/HAp-0.5	0.5	99.5	85
PLA/HAp-1.0	1.0	99.0	85
PLA/HAp-2.0	2.0	98.0	85
PLA/HAp-2.5	2.5	97.5	85
PLA/HAp-3.0	3.0	97.0	85

Membrane characterization

Fourier transform infrared spectroscopy

The chemical structure of the adsorptive membrane samples was studied using the Shimadzu (IRAfnity-1S) Fourier transform infrared spectrometer (FTIR) within a range of 400–4000 cm^{-1}. The membrane samples were held in place by a clamp and placed active-face down on ATR crystal.

Porosity, water content, and contact angle measurement

Porosity and water content of the membranes were determined by gravimetric method, using Eqs. (1) and (2):

$$\varepsilon\ (\%) = \frac{\left(w_w - w_d\right)/\rho_w}{\left(w_w - w_d\right)/\rho_w + \left(w_d/\rho_p\right)} \times 100 \tag{1}$$

$$\text{Water content}\ \ (\%) = \frac{W_w - W_d}{W_d} \times 100 \tag{2}$$

where ε denotes the membrane porosity, w_d and w_w are the weight of membrane in its dry and wet states, respectively; ρ_w is the density of water and ρ_p is the density of PLA. For each membrane, three samples were taken for porosity measurement and the average value was reported.

The hydrophilicity of the membranes was measured by a static surface contact angle goniometer (Jikan Company, Iran) at room temperature. The contact angle of each sample was measured at least five times at different places of the membrane and the mean value was reported.

Pure water flux and mechanical strength of the fabricated membranes

The pure water flux (PWF) was determined using a laboratory-scale submerged flat sheet filtration system with 15 cm^2 of membrane area (Etemadi and Qazvini 2020). The module was connected to a vacuum pump (0.8 bar), and water was filtered through the membrane and after reaching a steady-state, PWF is calculated using Eq. (3):

$$\mathrm{PWF} = \frac{V}{A \cdot t} \tag{3}$$

where V denotes the collected volume of water in L, A is the membrane area in m^2, and t is the processing time in h.

Mechanical properties of the membranes were measured using a tensile testing machine (STM-5, Iran). The membrane samples were cut into 50 mm in length and 10 mm in width and examined at an extension rate of 10 mm/min. The test was performed in triplicate, and the average of the results was calculated and reported.

Morphological studies

The surface and cross-sectional morphologies of the prepared membranes were studied by a field emission scanning electron microscopy (FE-SEM) (MIRA3 FEG-SEM, Tescan) equipped with an energy-dispersive X-ray (EDX) detector. Samples for cross-sectional evaluation were prepared by fracturing the flat sheets in liquid nitrogen. To analyze the surface roughness, atomic force microscope (AFM) (Nanosurf® Mobile S scanning probe-optical microscope, Switzerland) was used. Imaging was performed on a scan size of 5 µm × 5 µm tapping mode.

Adsorption and regeneration study

Static adsorption study of the fabricated membranes

The static adsorption of the PLA/HAp adsorptive membranes was tested by batch experiments where 0.2 g of the membranes with 15cm^2 area was immersed into a 200 mL of the synthetic water containing both Pb and As with concentration of 10, 5, 2, and 1 ppm. For kinetics analysis, the concentration of heavy metal solution was adjusted to 100 ppb for better comparison between batch and dynamic adsorption. The solutions were stirred for 48 h at 25 °C, and the heavy metal's concentrations in the solutions were quantified by atomic absorption spectrophotometer (Varian 220-Graphite Furnace). The desired pH of the solution was adjusted at 7.0 by 0.1 M HCl or 0.1 M NaOH solutions. The adsorption capacity and removal efficiency of the membranes for each cation and anion are calculated according to Eqs. (4)–(6):

$$q_t = \frac{(C_0 - C_t)V}{M_\mathrm{m}} \tag{4}$$

$$q_\mathrm{e} = \frac{(C_0 - C_\mathrm{e})V}{M_\mathrm{m}} \tag{5}$$

$$\text{Removal efficiency } (\%) = \frac{(C_0 - C_t)}{C_0} \times 100 \tag{6}$$

where C_t is the concentration of heavy metal ions at time t, C_o and C_e are the initial and equilibrium concentrations of the ions in the solution, respectively; V is the total volume of the solution, and M_m is the mass of dry membrane used in the adsorption study. q_e and q_t are the adsorption capacity at equilibrium and time t, respectively.

Dynamic adsorption study of the fabricated membranes

The dynamic adsorption performances of the fabricated membranes were evaluated by submerged filtration system with 200 mL of Pb and As heavy metal solution under different TMPs including 0.4, 0.6, and 0.8 bar. At certain intervals, the samples were withdrawn from the filtration system and the concentrations of heavy metals were determined. The membranes were regenerated by filtering 50 mL HCl and NaOH solutions (0.1 M) through the membrane, respectively. After regeneration, the second cycle of experiments for 200 mL solution was initiated and this trend was repeated for five cycles. The concentrations of heavy metals were determined according the procedure for the first cycle.

Results and discussion

Fourier transform infrared spectroscopy analysis

The FTIR spectra of the HAp powder, neat PLA membrane, and PLA/Hap-2.5 membrane as a representative of all other PLA/HAp adsorptive membranes are shown in Fig. 1. The scans depicted a slight difference between the spectra of the neat PLA membrane and the PLA/HAp adsorptive membrane. In the neat PLA membrane, the peak at 1753 cm^{-1} is assigned to the C=O stretching vibration where the presence of peaks at 2953, 2991 cm^{-1}, and 1082 cm^{-1} is corresponded to the C–H and C–O stretching, respectively (Rahman

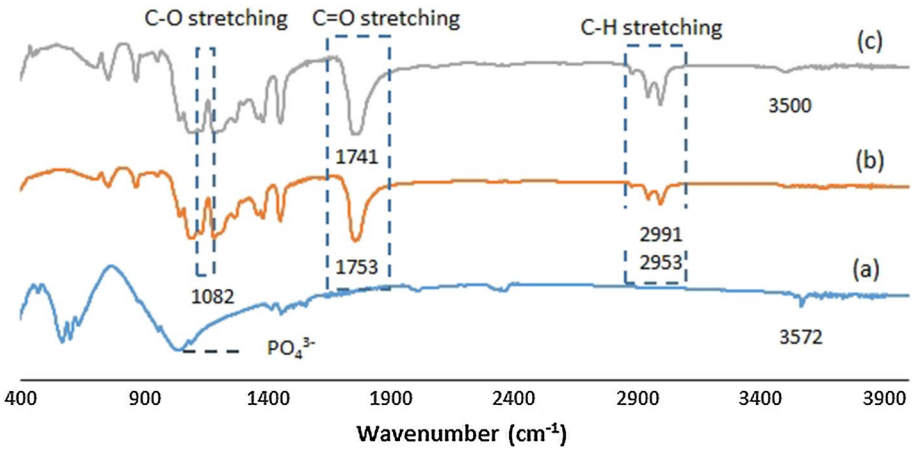

Fig. 1 FTIR spectra of **a** HAp, **b** neat PLA and **c** PLA/HAp-2.5 membranes

Table 2 Contact angle, porosity, and water content of neat and adsorptive PLA membranes

Membrane	Contact angle (°)	Porosity (%)	Water content (%)
PLA	85	58	59
PLA/HAp-1.0	79	62	63
PLA/HAp-2.0	68	69	70
PLA/HAp-2.5	57	78	85
PLA/HAp-3.0	45	53	109

et al. 2018). In spectra of PLA/HAp-2.5, the peak of the OH^- stretching bands of HAp at about 3572 cm^{-1} has been slightly shifted to lower wave number around 3500 cm^{-1}.

Also, the C–H band for the PLA/HAp-2.5 membrane showed a slight shift to lower wave numbers due to the occurrence of the P–O peak of PO_4^{3-} groups of the HAp in the same region of the spectra. It is noticeable that there is no distinct peak for P–O band in the adsorptive membrane because of the very close value of P–O and C–O spectrum (Persson et al. 2014).

Hydrophilicity, porosity, and water content of the fabricated membranes

Variation in the contact angle, porosity, and water content of each membrane with HAp concentration is presented in Table 2. The results showed that the contact angle of the membranes, as an indication of hydrophilicity, was reduced from 85° to 45° by addition of 3.0 wt% HAp nanoparticles into PLA matrix. As shown in Table 2, the addition of HAp improved the hydrophilicity of PLA/HAp membranes compared with pristine PLA membrane. This suggested that the growth in the number of surface OH groups with increasing HAp content was the key to the observed rise in hydrophilicity of the PLA-based absorptive membranes.

Porosity results revealed that the porosity of PLA-based membrane increased from 58 to 78% with increasing concentration of HAp from 0 to 2.5 wt%. It was observed that

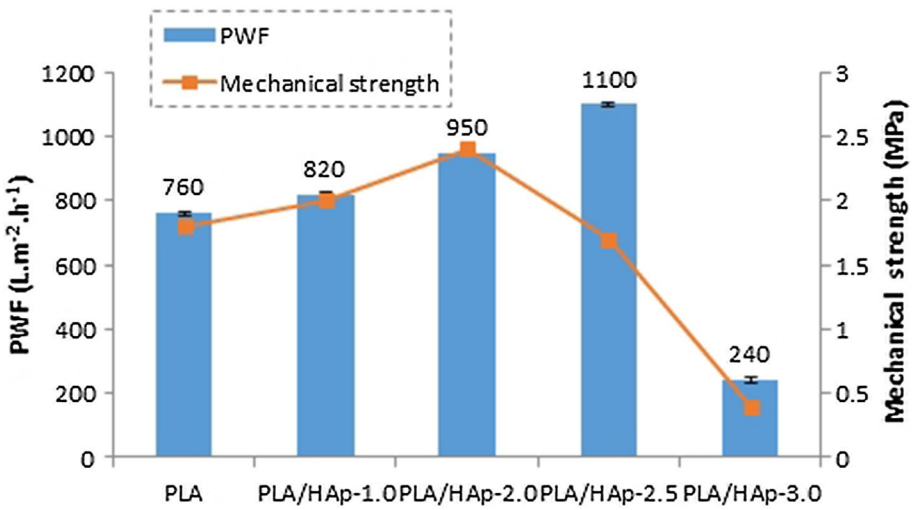

Fig. 2 PWF and mechanical strength of neat and PLA adsorptive membranes

further addition of HAp led to lower porosity rooted from membrane pores clogging accompanied with agglomerated nanoparticles. Water content test results indicated that water uptake of membranes enhanced by increasing the HAp content of the membranes up to 3.0 wt%. This can be described by the mutual effect of HAp on membrane structure by increasing the hydrophilicity and pore blockage for PLA/HAp-3.0 membrane (Daraei et al. 2012).

Permeability and mechanical properties

Figure 2 shows the variation in the permeability and mechanical strength of PLA/HAp adsorptive membranes with HAp concentration. It can be observed that the pure water flux of the membranes increased from 760 to 1100 L m^{-2} h^{-1} by incorporating 2.5 wt% of HAp. This is a direct consequence of the increment in the porosity and hydrophilicity of the membranes. However, with the higher concentration of HAp (3.0 wt%), membrane porosity has a more dominant effect on permeability than surface hydrophilicity.

The variation in membranes' mechanical strength with HAp nanoparticle concentration is similar to the trend of porosity up to 2.0 wt% of HAp. To explain these results, membrane porosity, inherent stiffness of HAp, the dispersion state of HAp, and the interaction between HAp nanoparticles and PLA matrix were considered. High intrinsic stiffness of HAp and appropriate interaction between HAp and polymer matrix improve the mechanical properties of adsorptive membranes. Besides this, though, it is also imperative to bear in mind that the presence of higher content of HAp results in pore-clogging and nanofiller agglomeration which adversely affects mechanical properties. Therefore, incorporation of over 2.5 wt% of HAp can lead to a non-uniform dispersion of HAp nanoparticles or/and heterogeneous casting solution which eventually causes the observed sharp reduction in mechanical strength in PLA/HAp-3.0 membrane.

Surface roughness of the membranes

3D AFM images of all the membranes illustrated in Fig. 3a–d allow the qualitative analysis and quantitative determination of mean roughness (R_a). It was observed from AFM analysis that membrane roughness of the fabricated membranes increases with the incorporation of the higher amount of HAp in the membrane matrix. Accumulation of HAp nanoparticles on the membrane surface and formation of polymer nodules during the phase separation could attribute to an increase in the membrane roughness. Mean roughness of PLA, PLA/HAp-1.0, PLA/HAp-2.0, and PLA/HAp-2.5 is 50, 65, 82, and 106 nm, respectively. HAp as a hydrophilic nanoparticle has the tendency to migrate toward the interface of the membrane surface and the water used for phase inversion which leads to increment in roughness. It is noticeable that the surface roughness of PLA/HAp-2.5 membrane is much higher than the neat PLA membrane. It is well known that the addition of nanoparticles increases the viscosity of casting solution causing an interaction between polymer matrix and nanoparticles; this slows down the phase separation and formation of polymer nodules on the membrane surface. Consequently, in PLA/HAp-2.5, both above-noted effective factors can simultaneously increase the roughness of the membrane.

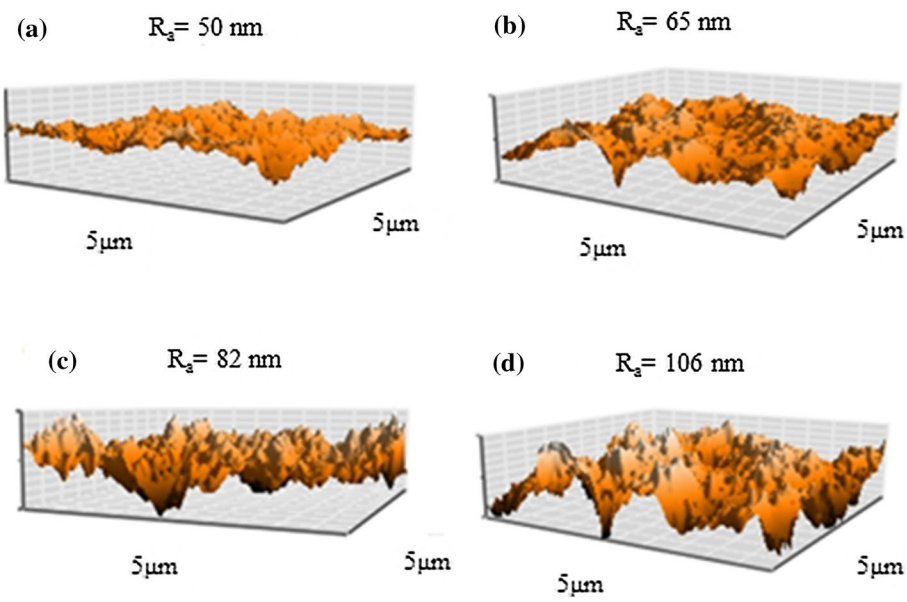

Fig. 3 AFM images of **a** neat PLA, **b** PLA/HAp-1.0, **c** PLA/HAp-2.0, **d** PLA/HAp-2.5 membranes

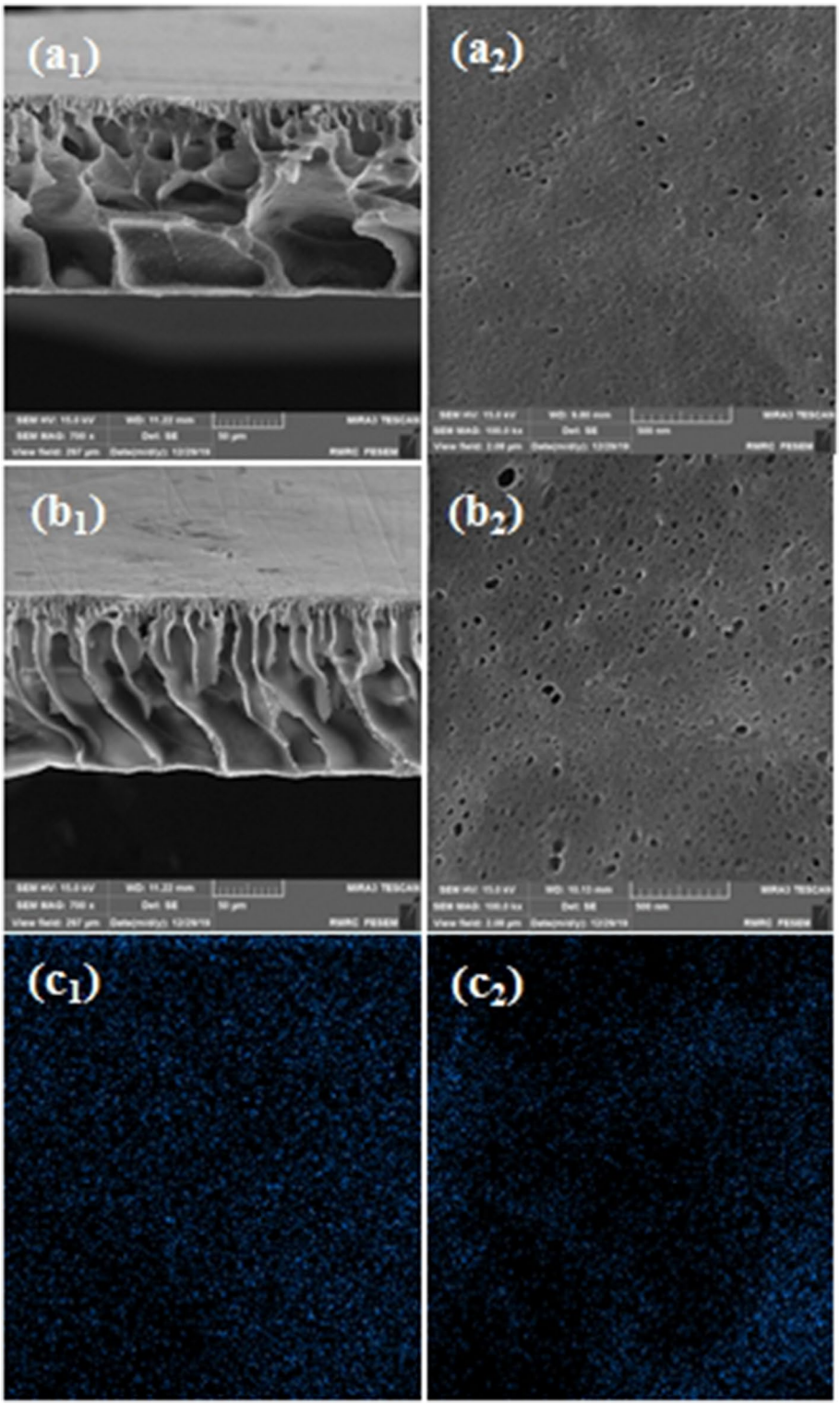

Fig. 4 FE-SEM images and elemental mappings (P) of cross section (left) and top surface (right) of **a** neat PLA and **b** PLA/HAp-2.5 membranes

Morphological analysis

The PLA/HAp-2.5 membrane was selected as an optimum membrane among other membranes according to higher permeability and acceptable mechanical properties. Figure 4 illustrates the surface and cross-sectional FE-SEM images of neat PLA and PLA/HAp-2.5 adsorptive membranes. Cross-sectional images exhibited asymmetric structure for both membranes with a dense top layer, finger-like structure, with several macrovoids at the sublayer. With the addition of

HAp, the finger-like structure extended straightly along the cross section of the membrane (Fig. 4a$_1$). Exchange kinetics and thermodynamic of phase separation have a significant influence on the membranes' structure. The addition of HAp nanoparticles leads to an increase in the thermodynamic instability and exchange rate of the solvent and non-solvent. This consequently brings about enlargement of the finger-like structure and a more porous structure of the membrane. These theories are firmly supported by the evidence obtained from surface FE-SEM images (Fig. 4b$_1$).

The top surface FE-SEM image of the neat PLA membrane (Fig. 4a$_2$) confirmed the presence of several pores (< 50 nm) distributed on the surface. With the addition of HAp (2.5 wt%), the number and sizes of the surface pores of the obtained membrane increased slightly (Fig. 4b$_2$). Generally, the increase in surface porosity with the addition of HAp can be attributed to the increase in the exchange rate of the solvent and non-solvent.

The surface and cross-sectional EDX map spectra of PLA/HAp-2.5 membrane are shown in Fig. 4c$_1$, c$_2$, respectively. The blue spots corresponding to phosphorus (P) show the uniform distribution of HAp in the surface and cross section of the membrane. It is evidenced from the EDX results that there is almost no significant difference between the dispersive map of P between the surface and cross section of the sample, indicative of practically uniform dispersion of HAp in the membrane.

Heavy metal adsorption study on PLA/HA membrane

Static adsorption

Isotherm analysis The Pb and As adsorption capacity of PLA and PLA/HAp-2.5 adsorptive membrane vs. the equilibrium concentrations of the heavy metal solutions are plotted in Fig. 5. The adsorption of Pb cations by the PLA/HAp-2.5 was ascribed to the coordination effects: (i) the phosphate functional group in the HAp could catch Pb cations via electrostatic interactions, and (ii) the substitution of Pb with Ca took place. The Pb adsorption capacity of the neat PLA membrane was attributed to the interaction between the carbonate group of PLA and Pb cations. However, the neat PLA membrane showed no adsorption capacity for As due to the absence of proper functional groups acting as an adsorbent in the membrane matrix. The As adsorption capacity of the adsorptive membranes is mainly due to the electrostatic interaction of Ca or Pb with oxyanions of As. Furthermore, there is a possibility of the replacement of As oxyanions with the phosphate group of HAp, however, it is negligible according to the literature (Nakahira et al. 2006). The adsorption capacity of the adsorptive membrane for Pb removal showed a substantial difference from that of As. The higher Pb adsorption capacity compared to As can be explained by the zeta potential of HAp (6.1) which is favora-

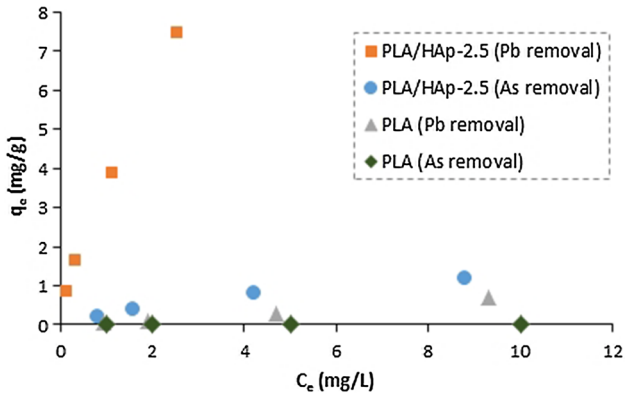

Fig. 5 Adsorption isotherms of Pb and As on PLA and PLA/HAp-2.5 membranes

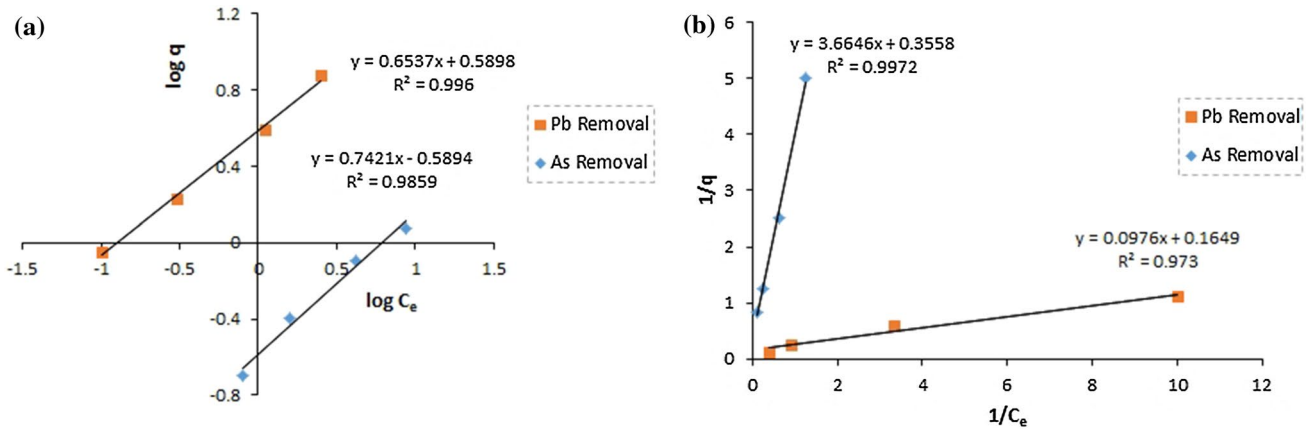

Fig. 6 Fitting curves for isotherm adsorption of Pb and As on PLA and PLA/HAp-2.5 membranes using **a** Langmuir and **b** Freundlich models

ble for the positively charged adsorption process (Lazarevic et al. 2008).

In addition, all the prepared membranes presented an increasing trend in Pb and As adsorption capacity by increasing heavy metal concentrations in the solution. This could be directly related to the higher chance of the adsorption interaction between ions and functional groups.

The adsorption equilibrium of Pb and As ions onto the prepared membranes was theoretically modeled using Langmuir and Freundlich equilibrium isotherm models. The linear forms of both models are presented in Eqs. (7) and (8):

$$\frac{1}{q} = \frac{1}{K_L C_e q_{max}} + \frac{1}{q_{max}} \tag{7}$$

$$\log q = \log K_F + \frac{1}{n} \log C_e \tag{8}$$

where q is the equilibrium adsorbed amount of metal ion, q_{max} is the maximum adsorption capacity (mg/g), K_L is the Langmuir adsorption capacity (L/mg), C_e is the heavy metals equilibrium concentration in solution (mg/L). K_F is the Freundlich constant, and n is the heterogeneity factor.

Figure 6 depicts linear plots of Langmuir and Freundlich isotherms for the adsorption of heavy metal ions on the PLA/HAp adsorptive membrane. In Fig. 6a, the Freundlich isotherm fits the Pb adsorption data well with high correlation coefficients. The Pb adsorption behavior may result from the adsorption mechanism on the heterogeneous surface of the adsorptive membrane which originates from functional groups of both HAp and PLA. In contrast, the experimental data for As correlate better with the Langmuir model with homogeneous adsorption sites (Fig. 6b).

Kinetics analysis The effect of the contact time on the removal efficiency of heavy metals and their residual

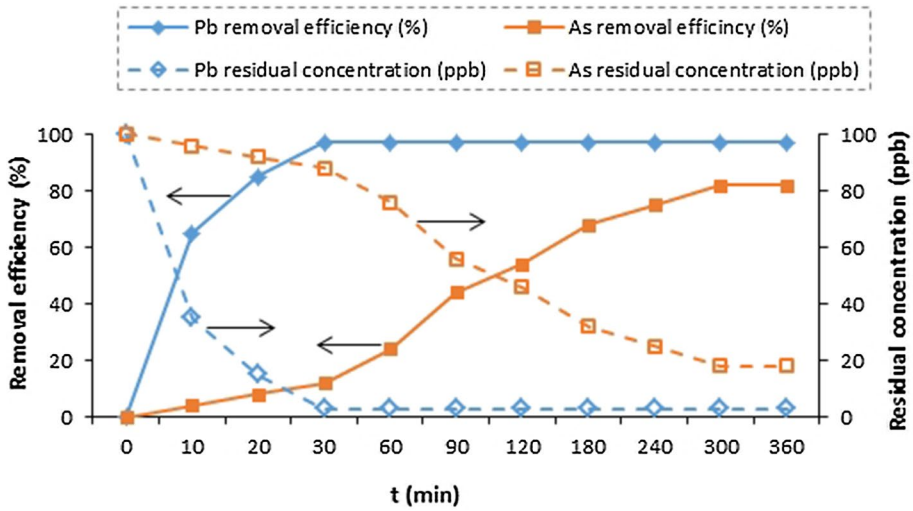

Fig. 7 Effect of contact time on the removal efficiency and residual concentration of Pb and As on PLA and PLA/HAp-2.5 membranes

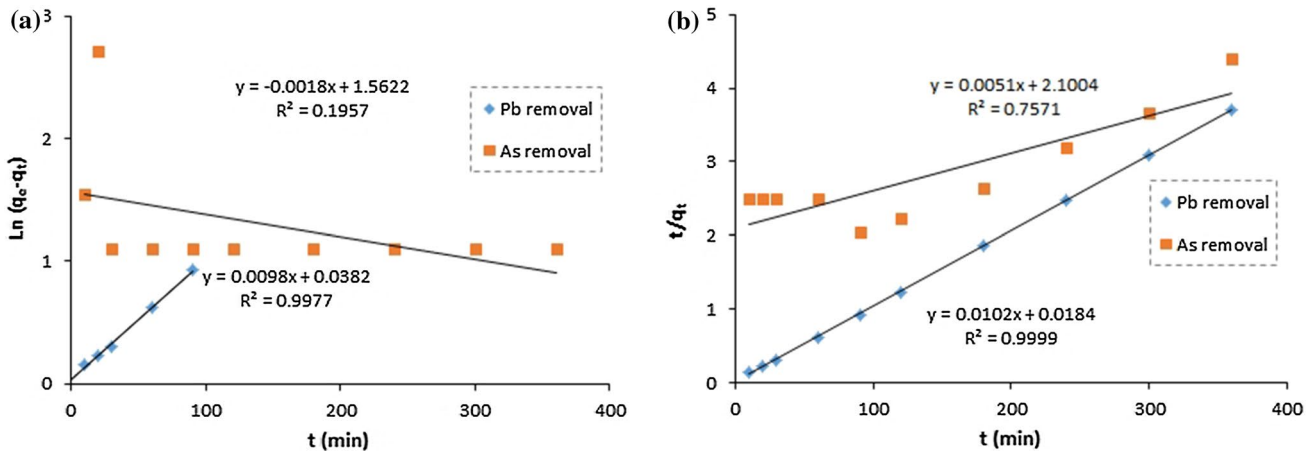

Fig. 8 Fitting curves for adsorption kinetics of Pb and As on PLA and PLA/HAp-2.5 membranes **a** pseudo-first-order and **b** pseudo-second-order models

concentrations in the 100 ppb aqueous solution for PLA/HAp-2.5 adsorptive membrane is presented in Fig. 7. It demonstrated that the removal efficiency of heavy metals significantly increased as the contact time increases. Interestingly, the adsorption rate of both ions was rapid at the initial stage and gradually slowed down afterward for both heavy metal ions. 97% Pb removal efficiency was achieved within the first 30 min, whereas the adsorption rate of As is lower than Pb and the maximum removal efficiency (82%) was gained after 5 h.

To investigate the adsorption rates of Pb and As ions, kinetic modeling of the adsorption was accomplished by the pseudo-first-order and pseudo-second-order models as follows:

$$\mathrm{Ln}\left(q_e - q_t\right) = \mathrm{Ln}q_e - k_1 t \tag{9}$$

$$\frac{t}{q_t} = \frac{1}{k_2 q_e^2} + \frac{t}{q_e} \tag{10}$$

where q_e and q_t are the adsorption capacity of heavy metals at equilibrium and time t, and k_1 and k_2 are the first- and second-order rate constants, respectively. The plots of $\mathrm{Ln}(q_e - q_t)$ and t/q versus t for the first- and second-order models are given in Fig. 8. Based on the correlation (R^2) given on the visual assessment of the plots in Fig. 8, it can be concluded that the pseudo-second-order kinetic model can provide appropriate fitness to Pb adsorption, whereas the opposite applies for As. It means that the adsorption process involved chemisorption between Pb metal ion and HAp, while the physical adsorption is predominant for As adsorption.

Dynamic adsorption and effects of regeneration cycles

As discussed earlier, since PLA/HAp-2.5 membrane was the best-performed one, it was selected for the dynamic adsorption investigations of Pb and As heavy metal ions. The PWF and removal efficiency of Pb and As heavy metal ions as a function of TMP, 0.4, 0.6, and 0.8 bar are depicted in Fig. 9a. As shown, the permeate flux increased remarkably by applying a higher amount of TMP, and the removal efficiency of both heavy metals showed a downward trend by increasing the TMP. Accordingly, the maximum removal efficiency of the heavy metal ions occurred at 0.4 bar which was 100% and 93% for Pb and As, respectively. The dynamic adsorption process at lower TMP allows benefiting all active sites of the adsorbent which leads to the maximum removal efficiency. In other words, the affinity of PLA/HAp absorptive membranes for heavy metal ions is inversely proportional to the employed TMP. On the other hand, the increase in As removal efficiency was more pronounced when the TMP was decreased. This may be attributed to the fact that slow filtration can improve the physical metal adsorption capacities.

The separation and regeneration performance of the selected membrane in the removal of Pb and As was evaluated at 0.4 bar for multiple adsorption–desorption consequent cycles, and the obtained results are represented in Fig. 9b. It was shown that the removal efficiency of Pb stayed constant at 100% for three filtration cycles and then reduced gradually. Moreover, comparing this figure to the experimental data indicated in Fig. 7 revealed that the removal efficiency of the dynamic adsorption is higher than the batch equilibrium adsorption. These results denoted that the adsorptive membrane allows the use of all active adsorption sites of the adsorbent, by taking the advantage of the convective flow compared to slow diffusion mechanisms in the batch adsorption.

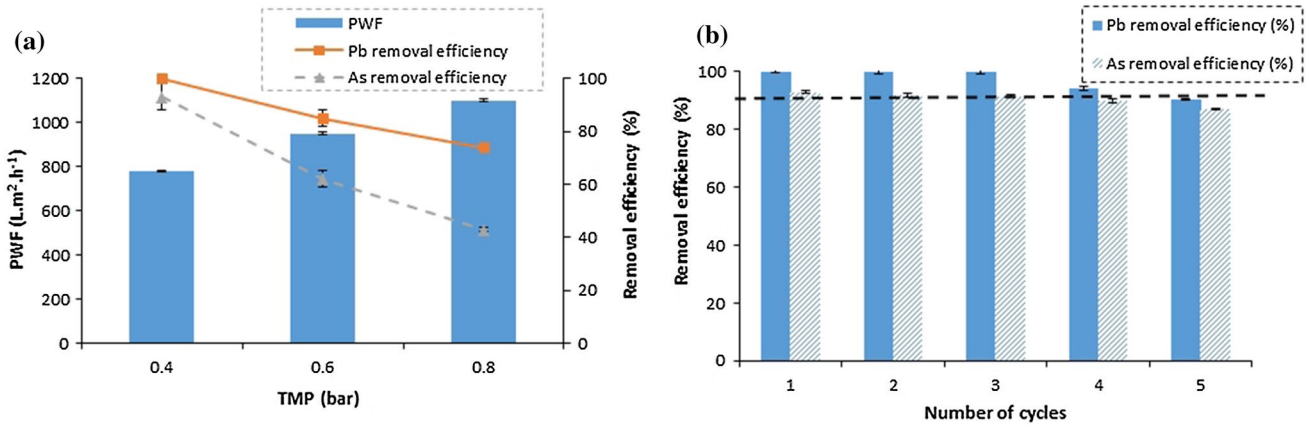

Fig. 9 **a** Effect of TMP on the PWF and removal efficiency of Pb and As on PLA/HAp-2.5 membrane, **b** removal efficiency of Pb and As in five adsorption/desorption cycles for PLA/HAp-2.5 membrane at TMP = 0.4 bar

Table 3 Comparison of maximum Pb and As removal efficiencies for different HAp adsorbents

Adsorbent	pH	Pb removal (%)	As removal (%)	Method	References
Hydroxyapatite	8.5	–	50	Batch adsorption	Mirhosseini et al. (2014)
Copper doped hydroxyapatite	7.0	–	35	Precipitation	Jahan et al. (2017)
Modified hydroxyapatite with SiO_2	8.5	–	90	Batch adsorption	Nakahira et al. (2006)
Cellulose-carbonated hydroxyapatite	7.0	–	88	Batch adsorption	Islam et al. (2011)
CA–hydroxyapatite composite	7.0	95	–	Batch adsorption	Hamad et al. (2020)
Chitosan–hydroxyapatite composite nanofiber	7.0	72	–	Batch adsorption	Aliabadi et al. (2014)
Fish scale-extracted chitosan–hydroxyapatite	2.0	75	–	Batch adsorption	Liaw et al. (2020)
Fish scale-extracted chitosan–hydroxyapatite	2.0	94	–	Fixed bed adsorption	Liaw et al. (2020)
Current work	7.0	100	93	Adsorptive membrane	

After five cycles, the removal efficiency of Pb dropped lower than 90% which led to maintaining the Pb concentration of the permeate solution below the MCL of 10 ppb. However, in the case of As ion, the removal efficiency decreased from 93 to 90% after four multiple adsorption–desorption cycles. It is obvious that the decrease in removal efficiencies of Pb is more noticeable than As after several regeneration cycles due to the chemical adsorption of Pb

For the sake of comparison, the results of some available studies toward the heavy metal ions removal by HAp as adsorbent are gathered and given with that of PLA/HAp membrane (current work) in Table 3. Since the initial concentration of heavy metals strongly increases the adsorption capacity, a direct comparison among different situations and getting a solid conclusion is somehow unachievable. Nonetheless, the priority of this work was set to compare the removal efficiency of different HAp nanoparticles or composites at low initial concentrations of Pb and As which are common in both surface or ground waters (≈ 100 ppb). According to the comparison results given in Table 3, it was evidenced that the PLA/HAp membrane exhibited the high-performance efficiency in removing both Pb and As ions from the aqueous solutions. Therefore it can be concluded that adsorptive membrane possesses higher adsorption capacity than other available HAp adsorbents in batch or column adsorption and the presence of Pb can improve the As adsorption capacity of HAp.

Conclusion

Efficient adsorptive membranes for simultaneous absorption of both cationic and anionic heavy metals from contaminated water were developed based on PLA biopolymer. The incorporation of 2.5 wt% of HAp as an adsorbent into PLA matrix was confirmed to be an effective approach to provide favorable permeability (1100 L m^{-2} h^{-1}), porosity (78%), and hydrophilicity (with a contact angle of 57°), excellent mechanical properties (strength of 1.7 MPa), and high Pb and As removal efficiency of the product membrane from contaminated water. The high adsorption capacity of the membrane was mainly attributed to the complexation between the metal ion and phosphate functional group in HAp via electrostatic interactions. Moreover, electrostatic interaction of Ca or Pb with oxyanions of As is found to be the origin of the As adsorption into the membrane. In the dynamic adsorption process, efficiency of Pb and As, from water, increased with reducing applied TMP. The PLA/HAp absorptive membranes showed excellent results for heavy metal ion removal at several consecutive cycles, however, the membrane performance retention in removal efficiency was higher for Pb ion. For PLA/HAp-2.5 membrane, the full removal efficiency of Pb was kept up to three adsorption-regeneration cycles, while a slight deterioration in As removal performance of the membrane was observed even in three cycles. Overall, it is worth noting that the proposed PLA/HAp membranes may

offer several advantages due to their bifunctional properties in removing both cationic and anionic heavy metal ions from aqueous solutions over the available membranes.

Acknowledgements The authors would like to express their appreciation to Water and Wastewater Company's Laboratory of East Azarbaijan and University of Bonab for the partial support of this study.

Funding This research work did not receive any specific grant from funding agencies in the public or commercial sectors.

Data availability All the data that support the findings of this study are available from the corresponding author upon request through email.

Declaration

Conflict of interest The authors declare that they have no conflict of interest.

References

Abdullah N, Gohari RJ, Yusof N, Ismail AF, Juhana J, Lau WJ, Matsuura T (2016) Polysulfone/hydrous ferric oxide ultrafiltration mixed matrix membrane: preparation, characterization and its adsorptive removal of lead(II) from aqueous solution. Chem Eng J 289:28–37

Aliabadi M, Irani M, Ismaeili J, Najafzadeh S (2014) Design and evaluation of chitosan/hydroxyapatite composite nanofiber membrane for the removal of heavy metal ions from aqueous solution. J Taiwan Inst Chem Eng 45:518-526. https://doi.org/10.1016/j.jtice.2013.04.016

Al-Wafi R, Ahmed MK, Mansour SF (2020) Tuning the synthetic conditions of graphene oxide/magnetite/hydroxyapatite/cellulose acetate nanofibrous membranes for removing Cr(VI), Se(IV) and methylene blue from aqueous solutions. J Water Process Eng 38:101543. https://doi.org/10.1016/j.jwpe.2020.101543

Anutrasakda W, Phasuk A, Tangku C (2020) Effect of different CO_3^{2-} to PO_4^{3-} molar ratios on the properties, morphology, and Pb(II) removal performance of carbonated hydroxyapatite. J Environ Chem Eng 9:104658. https://doi.org/10.1016/j.jece.2020.104658

Anwar F, Arthanareeswaran G (2019) Silver nano-particle coated hydroxyapatite nano-composite membrane for the treatment of palm oil mill effluent. J Water Process Eng 31:100844. https://doi.org/10.1016/j.jwpe.2019.100844

Campisi S, Evangelisti C, Postole G, Gervasini A (2021) Combination of interfacial reduction of hexavalent chromium and trivalent chromium immobilization on tin-functionalized hydroxyapatite materials. Appl Surf Sci 539:148227. https://doi.org/10.1016/j.apsusc.2020.148227

Chatterjee S, De S (2015) Adsorptive removal of arsenic from groundwater using a novel high flux polyacrylonitrile (PAN)–laterite mixed matrix ultrafiltration membrane. Environ Sci Water Res Technol 1:227–243. https://doi.org/10.1039/C4EW00075G

Chon H, Ohandja D, Voulvoulis N (2010) Implementation of e.U. Water framework directive: source assessment of metallic substances at catchment levels. J Environ Monit 12:33–47

Chuan D, Fan R, Wang Y, Ren Y, Wang C, Du Y, Zhou L, Yu J, Gu Y, Chen H, Guo G (2020) Stereocomplex poly(lactic acid)-based composite nanofiber membranes with highly dispersed hydroxyapatite for potential bone tissue engineering. Compos Sci Technol 192:108107. https://doi.org/10.1016/j.compscitech.2020.108107

Corami A, Mignardi S, Ferrini V (2008) Cadmium removal from single- and multi-metal (Cd + Pb + Zn + Cu) solutions by sorption on hydroxyapatite. J Colloid Interface Sci 317(2):402–408. https://doi.org/10.1016/j.jcis.2007.09.075

Czerniczyniec M, Farías S, Magallanes J, Cicerone D (2007) Arsenic(V) adsorption onto biogenic hydroxyapatite: solution composition effects. Water Air Soil Pollut 180:75–82. https://doi.org/10.1007/s11270-006-9251-6

Damodar RA, You SJ, Chou HH (2009) Study the self cleaning, antibacterial and photocatalytic properties of TiO_2 entrapped pvdf membranes. J Hazard Mater 172:1321–1328

Daraei P, Madaeni SS, Ghaemi N, Salehi E, Khadivi MA, Moradian R, Astinchap B (2012) Novel polyethersulfone nanocomposite membrane prepared by PANI/Fe_3O_4 nanoparticles with enhanced performance for Cu(II) removal from water. J Membr Sci 415–416:250–259

de Resende NS, Camargo CLM, Reis PC, Perez CAC, Salim VMM (2019) Mechanisms of mercury removal from aqueous solution by high-fixation hydroxyapatite sorbents. Int J Sci Environ Technol 16(11):7221–7228. https://doi.org/10.1007/s13762-019-02401-8

Deng L, Li Y, Zhang A, Zhang H (2020) Nano-hydroxyapatite incorporated gelatin/zein nanofibrous membranes: fabrication, characterization and copper adsorption. Int J Biol Macromol 154:1478–1489. https://doi.org/10.1016/j.ijbiomac.2019.11.029

Dixit S, Hering JG (2003) Comparison of Arsenic(V) and Arsenic(III) sorption onto iron oxide minerals: implications for arsenic mobility. Environ Sci Technol 37:4182–4189

Etemadi H, Qazvini H (2020) Investigation of alumina nanoparticles role on the critical flux and performance of polyvinyl chloride membrane in a submerged membrane system for the removal of humic acid. Polym Bull 78:2645–2662. https://doi.org/10.1007/s00289-020-03234-z

Fang X, Zhu S, Ma J, Wang F, Xu H, Xia M (2020) The facile synthesis of zoledronate functionalized hydroxyapatite amorphous hybrid nanobiomaterial and its excellent removal performance on Pb^{2+} and Cu^{2+}. J Hazard Mater 392:122291. https://doi.org/10.1016/j.jhazmat.2020.122291

Foroughi F, Hassanzadeh-Tabrizi SA, Amighian J, Saffar-Teluri A (2015) A designed magnetic $CoFe_2O_4$–hydroxyapatite core–shell nanocomposite for Zn(II) removal with high efficiency. Ceram Int 41(5, Part B):6844–6850. https://doi.org/10.1016/j.ceramint.2015.01.133

Fu F, Wang Q (2011) Removal of heavy metal ions from wastewaters: a review. J Environ Manag 92:407–418

Fu Y, Zhang J, Lin H, Mo A (2021) 2d titanium carbide(mxene) nanosheets and 1d hydroxyapatite nanowires into free standing nanocomposite membrane: in vitro and in vivo evaluations for bone regeneration. Mater Sci Eng C 118:111367. https://doi.org/10.1016/j.msec.2020.111367

Gopalakannan V, Periyasamy S, Viswanathan N (2018) Fabrication of magnetic particles reinforced nano-hydroxyapatite/gelatin composite for selective Cr(VI) removal from water. Environ Sci Water Res Technol 4:783–794. https://doi.org/10.1039/C8EW00027A

Hamad AA, Hassouna MS, Shalaby TI, Elkady MF, Elkawi MAA, Hamad HA (2020) Electrospun cellulose acetate nanofiber incorporated with hydroxyapatite for removal of heavy metals. Int J Biol Macromol 151:1299–1313. https://doi.org/10.1016/j.ijbiomac.2019.10.176

Hokkanen S, Bhatnagar A, Repo E, LouSillanpää SM (2016) Calcium hydroxyapatite microfibrillated cellulose composite as a potential adsorbent for the removal of Cr(VI) from aqueous solution. Chem Eng J 283:445–452. https://doi.org/10.1016/j.cej.2015.07.035

Hubadillah SK, Othman MHD, Tai ZS, Jamalludin MR, Yusuf NK, Ahmad A, Rahman MA, Jaafar J, Kadir SHSA, Harun Z (2020) Novel hydroxyapatite-based bio-ceramic hollow fiber membrane derived from waste cow bone for textile wastewater treatment. Chem Eng J 379:122396. https://doi.org/10.1016/j.cej.2019.122396

Iniguez-Franco F, Auras R, Burgess G, Holmes D, Rubino M, Soto-Valdez H (2016) Concurrent solvent induced crystallization and hydrolytic degradation of PLA by water–ethanol solutions. Polymer 99:315–323. https://doi.org/10.1021/am4038432

Islam M, Mishra PC, Patel R (2011) Arsenate removal from aqueous solution by cellulose-carbonated hydroxyapatite nanocomposites. J Hazard Mater 189:755–763. https://doi.org/10.1016/j.jhazmat.2011.03.051

Jahan SA, Mollah MYA, Ahmed S, Susan MABH (2017) Copper-doped hydroxyapatite for removal of arsenic(v) from aqueous system. J Sci Res 9(4):383–402. https://doi.org/10.3329/JSR.V9I4.32606

Jiang H, Zuo Y, Zou Q, Wang H, Du J, Li Y, Yang X (2013) Biomimetic spiral-cylindrical scaffold based on hybrid chitosan/cellulose/nano-hydroxyapatite membrane for bone regeneration. Appl Mater Interfaces 5:12036–12044. https://doi.org/10.1021/am4038432

Jiang J, Long Y, Hu X, Hu J, Zhu M, Zhou S (2020) A facile microwave-assisted synthesis of mesoporous hydroxyapatite as an efficient adsorbent for Pb^{2+} adsorption. J Solid State Chem 289:121491. https://doi.org/10.1016/j.jssc.2020.121491

Kıranşan M, Khataee A, Karaca S, Sheydaei M (2015) Artificial neural network modeling of photocatalytic removal of a disperse dye using synthesized of ZnO nanoparticles on montmorillonite. Spectrochim Acta Part A Mol Biomol Spectrosc 140:465–473

Lazarevic S, Jankovic-Castvan I, Tanaskovic D, Pavicevic V, Janackovic D, Petrovic R (2008) Sorption of Pb^{2+}, Cd^{2+}, and Sr^{2+} ions on calcium hydroxyapatite powder obtained by the hydrothermal method. J Environ Eng 134(8):683–688. https://doi.org/10.1061/(ASCE)0733-9372

Lee A, Elamb JW, Darling SB (2016) Membrane materials for water purification: design, development, and application. Environ Sci Water Res Technol 2:17–42. https://doi.org/10.1039/C5EW00159E

Liaw B-S, Chang T-T, Chang H-K, Liu W-K, Chen P-Y (2020) Fish scale-extracted hydroxyapatite/chitosan composite scaffolds fabricated by freeze casting an innovative strategy for water treatment. J Hazard Mater 382:121082. https://doi.org/10.1016/j.jhazmat.2019.121082

Louihi S, Noukrati H, Tamraoui Y, Said HA, Ben Youcef H, Manoun B, Barroug A (2020) Adsorption and structural properties of hydroxy and new lacunar apatites. J Mol Struct 1202:127225. https://doi.org/10.1016/j.molstruc.2019.127225

Manica M, Battistelli AA, Belli TJ, Souza JB, Lapolli FR, Vidal CMS (2020) Effects of electrocoagulation on membrane fouling and treatment performance of a membrane bioreactor operated without sludge discharge. Int J Sci Environ Technol 18:1695–1708. https://doi.org/10.1007/s13762-020-02953-0

Mirhosseini M, Biazar E, Saeb K (2014) Removal of arsenic from drinking water by hydroxyapatite nano particles. Curr World Environ 9(2):331–338. https://doi.org/10.12944/CWE.9.2.13

Moriya A, Shen P, Ohmukai Y, Maruyama T, Matsuyama H (2012) Reduction of fouling on poly(lactic acid) hollow fiber membranes by blending with poly(lactic acid)–polyethylene glycol–poly(lactic acid) triblock copolymers. J Membr Sci 415–416:712–717. https://doi.org/10.1016/j.memsci.2012.05.059

Nakahira A, Okajima T, Honma T, Yoshioka S, Tanaka I (2006) Arsenic removal by hydroxyapatite-based ceramics. Chem Lett 35(8):856–857. https://doi.org/10.1246/cl.2006.856

Naseem R, Tahir SS (2001) Removal of Pb(II) from aqueous/acidic solutions by using bentonite as an adsorbent. Water Res 35:3982–3986

Pandele AM, Comanici FE, Carp CA, Miculescu F, Voicu SI, Thakur VK, Serban BC (2017) Synthesis and characterization of cellulose acetate–hydroxyapatite micro and nano composites membranes for water purification and biomedical applications. Vacuum 146:599–605. https://doi.org/10.1016/j.vacuum.2017.05.008

Persson M, Lorite GS, Kokkonen HE, Cho SW, Lehenkari PP, Skrifvars M, Tuukkanen J, Sebastiano C (2014) Effect of bioactive extruded PLA/HA composite films on focal adhesion formation of preosteoblastic cells. Colloids Surf B 121:409–416. https://doi.org/10.1016/j.colsurfb.2014.06.029

Pooladi A, Bazargan-Lari R (2020) Simultaneous removal of copper and zinc ions by chitosan/hydroxyapatite/nano-magnetite composite. J Mater Res Technol 9(6):14841–14852. https://doi.org/10.1016/j.jmrt.2020.10.057

Rahman MM, Islam MS, Li GS (2018) Development of pla/cs/zno nanocomposites and optimization its mechanical, thermal and water absorption properties. Polym Test 68:302–308. https://doi.org/10.1016/j.polymertesting.2018.04.026

RoyChoudhury P, Majumdar S, Sarkar S, Kundu B, Sahoo GC (2019) Performance investigation of Pb(II) removal by synthesized hydroxyapatite based ceramic ultrafiltration membrane: Bench scale study. Chem Eng J 355:510–519. https://doi.org/10.1016/j.cej.2018.07.155

Saoiabi S, Achelhi K, Masse S, Saoiabi A, Laghzizil A, Coradin T (2013) Organo-apatites for lead removal from aqueous solutions: a comparison between carboxylic acid and aminophosphonate

surface modification. Colloids Surf A Physicochem Eng Asp 419:180–185. https://doi.org/10.1016/j.colsurfa.2012.12.005

Sheha RR, Moussa SI, Attia MA, Sadeek SA, Someda HH (2016) Novel substituted hydroxyapatite nanoparticles as a solid phase for removal of Co(II) and Eu(III) ions from aqueous solutions. J Environ Chem Eng 4(4, Part A):4808–4816. https://doi.org/10.1016/j.jece.2016.11.005

Sogaard E (2014) Advanced arsenic removal technologies review. In: Sogaard E (ed) Chemistry of advanced environmental purification processes of water. Elsevier, Aalborg, pp 299–300

Song H, Carraway ER, Kim YH, Batchelor B, Jeon B-H, Kim J-G (2008) Amendment of hydroxyapatite in reduction of tetrachloroethylene by zero-valent zinc: its rate enhancing effect and removal of Zn(II). Chemosphere 73(9):1420–1427. https://doi.org/10.1016/j.chemosphere.2008.08.006

Thanh DN, Novak P, Vejpravova J, Vu HN, Lederer J, Munshi T (2018) Removal of copper and nickel from water using nanocomposite of magnetic hydroxyapatite nanorods. J Magn Magn Mater 456:451–460. https://doi.org/10.1016/j.jmmm.2017.11.064

Tomar G, Thareja A, Sarkar S (2015) Enhanced fluoride removal by hydroxyapatite-modified activated alumina. Int J Sci Environ Technol 12(9):2809–2818. https://doi.org/10.1007/s13762-014-0653-5

Uddin MT, Mozumder MSI, Islam MA, Deowan SA, Hoinkis J (2007) Nanofiltration membrane process for the removal of arsenic from drinking water. Chem Eng Technol 30(9):1248–1254

Viipsi K, Sjoberg S, Tonsuaadu K, Shchukarev A (2013) Hydroxy- and fluorapatite as sorbents in Cd(II)–Zn(II) multi-component solutions in the absence/presence of EDTA. J Hazard Mater 252–253:91–98. https://doi.org/10.1016/j.jhazmat.2013.02.034

Yang H, Masse S, Rouelle M, Aubry E, Li Y, Roux C, Journaux Y, Li L, Coradin T (2015) Magnetically recoverable iron oxide–hydroxyapatite nanocomposites for lead removal. Int J Sci Environ Technol 12(4):1173–1182. https://doi.org/10.1007/s13762-014-0514-2